Passive Driver Gaze Tracking with Active Appearance Models

Takahiro Ishikawa, Simon Baker,
Iain Matthews, and Takeo Kanade

CMU-RI-TR-04-08

Passive Driver Gaze Tracking with Active Appearance Models

CMU-RI-TR-04-08

Takahiro Ishikawa, Simon Baker, Iain Matthews and Takeo Kanade

The Robotics Institute
Carnegie Mellon University

Abstract

Passive gaze estimation is usually performed by locating the pupils, and the inner and outer eye corners in the image of the driver's head. Of these feature points, the eye corners are just as important, and perhaps harder to detect, than the pupils. The eye corners are usually found using local feature detectors and trackers. In this paper, we describe a passive driver gaze tracking system which uses a global head model, specifically an Active Appearance Model (AAM), to track the whole head. From the AAM, the eye corners, eye region, and head pose are robustly extracted and then used to estimate the gaze.

1 Introduction

An intelligent car that monitors the behavior of the driver can be made far safer. Many of the most important components of the driver's behavior are related to their eye gaze. Whether the driver is drowsy or not is related to both their blink rate and their temporal gaze variation. Whether they are distracted or not can often be determined from detecting whether they are looking outside into the road scene, or instead at other passengers, the car radio, etc. By combining eye gaze with an understanding of the objects in the road-scene, it is even possible for an intelligent car to determine whether the driver has noticed potential dangers in the scene.

Most passive approaches to gaze estimation are in essence very similar. See, for example, [3–5, 7, 9, 10]. The location of the pupil (or equivalently the iris), together with the inner and outer

corners of the eye, are detected in the input image(s). The eye gaze can then be computed using a simple geometric head model. If an estimate of the head pose is available, a more refined geometric model can be used and a more accurate gaze estimate made.

Of these four quantities (iris/pupil location, inner eye corner location, outer eye corner location, and head pose), the most difficult to estimate reliably are the eye corners (and to a lesser extent the head pose.) Once the eye corners have been located, locating the iris/pupil, both robustly and accurately, is relatively straightforward. Perhaps somewhat ironically, the main difficulty in gaze estimation is not finding the iris/pupil.

The usual approach to locating the inner and outer eye corners is feature point detection and tracking [4, 5]. The head pose is normally computed in a similar manner; i.e. first detect and track a collection of anatomical feature points (eye corners, nose, etc) and then use a simple geometric model to compute the head pose. The problem with all of these feature-based methods is that they are very local; they only use information in the immediate vicinity of the feature point. If the face was tracked as a single object, a lot more visual information could be used to detect and track the eye corners and estimate the head pose, both more robustly and more accurately.

In recent years, a number of face models have been proposed to model the face as a single object, most notably Active Appearance Models (AAMs) [2] and 3D Morphable Models (3DMMs) [1]. Unfortunately, AAMs are only 2D models and so estimating the 3D head pose is difficult. On the other hand, fitting or tracking with 3D models is relatively slow. In particular, the fastest algorithm [8] to track with a 3DMM operates at around 30 seconds per frame (i.e. almost 1000 times slower than real-time, by which we mean 30 frames per second).

Recently, we have developed real-time algorithms for fitting both 2D AAMs [6] and a 3D variant of them [11]. Both of these algorithms operate at well over 200 frames per second, leaving plenty of time for the other computational tasks, such as iris/pupil detection, and the estimation of the gaze direction itself. In this paper, we describe how we have used these algorithms to build a gaze estimation system that derives its robustness and high accuracy from the fact that the eye corners and head pose are estimated using the entire appearance of the face, rather than by just

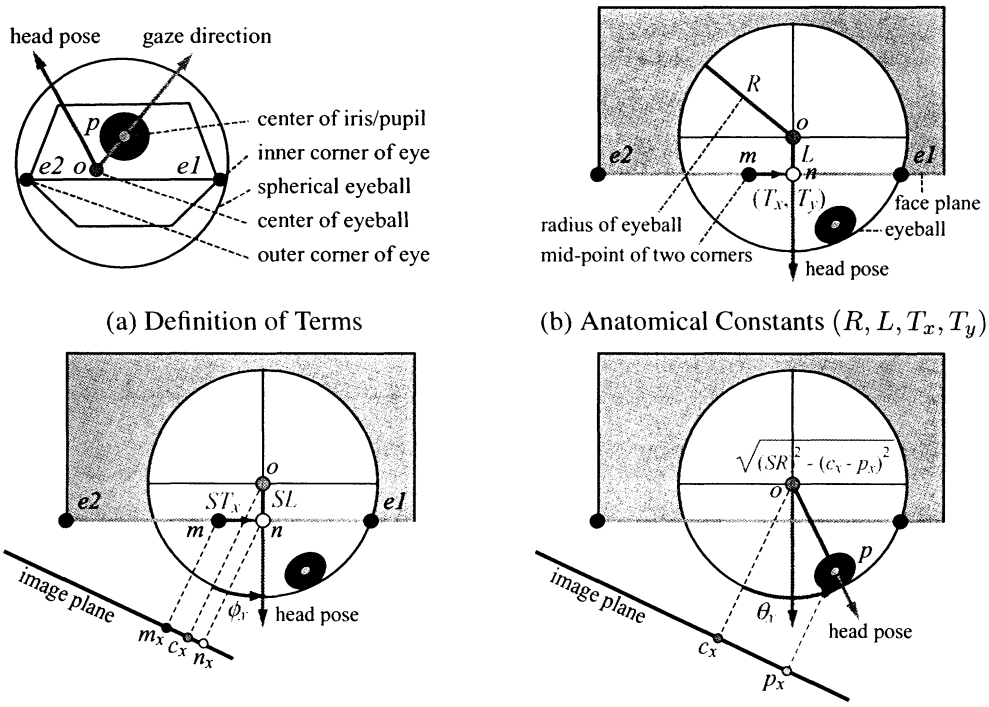

(a) Definition of Terms

(b) Anatomical Constants (R, L, T_x, T_y)

(c) Top down view for computing the offsets to the eye center using the head pose ϕ_x

(d) Top down view of the eyeball used for computing the gaze direction θ_x

Figure 1: Gaze Estimation Geometric Model (a) In the image we detect the pupil and the eye corners (using the AAM.) From these quantities we first estimate the eyeball center and radius, and then the gaze. (b) The anatomical constants (R_0, L, T_x, T_y). (c) Top down view used to compute the offsets to the eye center from the head pose ϕ_x. (d) To down view used to compute the gaze direction θ_x.

tracking a few isolated feature points.

2 Gaze Estimation Geometric Model

We begin by describing the geometric head model we use to estimate the gaze direction. There is nothing particularly novel about this model. Similar models have been used by other authors [4,5]. The essence of our model is contained in Figure 1. We assume that the eyeball is spherical and that the inner and outer eye corners have been estimated, in our case using an AAM as described in the following section. Our algorithm can be split into two steps:

1. Estimate (1) the center and (2) the radius of the eyeball in the image from the eye corners

and the head pose.

2. Estimate the gaze direction from the pupil location, the center and radius of the eyeball.

The first of these steps requires the following anatomical constants, also shown in Figure 1(b):

- R_0: The radius of the eyeball in the image when the "scale" of the face is 1 (see below for a definition of scale).
- (T_x, T_y): The offset in the image (when the face is frontal and the "scale" is 1) between the mid-point of the two eye corners and the center of the eyeball.
- L: The depth of the center of the eyeball relative to the plane containing the eye corners.

We now describe these two steps in turn and then how to estimate the anatomical constants.

2.0.1 Estimating the Center and Radius of the Eyeball

The center and radius of the eyeball are computed using the following three steps:

1. The mid-point (m_x, m_y) between the inner corner $(e1_x, e1_y)$ and outer corner $(e2_x, e2_y)$ is computed:

$$\begin{pmatrix} m_x \\ m_y \end{pmatrix} = \begin{pmatrix} \frac{e1_x+e2_x}{2} \\ \frac{e1_y+e2_y}{2} \end{pmatrix}. \quad (1)$$

2. The scale of the face S is computed. The most obvious way to estimate the scale is to use the foreshorten-corrected distance between the eye corners:

$$S = \frac{\sqrt{(e1_x - e2_x)^2 + (e1_y - e2_y)^2}}{\cos \phi_x} \quad (2)$$

The disadvantage of this approach is that it is very noise sensitive because it is the difference between two points that are very close together in the image. Instead, we used the scale that is estimated by the AAM. This estimate is more reliable because the scale is computed by effectively averaging over the entire face region.

3. The center of the eyeball (o_x, o_y) is then computed as the mid-point (m_x, m_y) plus two corrections:

$$\begin{pmatrix} o_x \\ o_y \end{pmatrix} = \begin{pmatrix} m_x \\ m_y \end{pmatrix} + S \begin{pmatrix} T_x \cos\phi_x \\ T_y \cos\phi_y \end{pmatrix} + SL \begin{pmatrix} \sin\phi_x \\ \sin\phi_y \end{pmatrix}. \tag{3}$$

The first correction is a foreshortened offset that compensates for the fact that the mid-point of the eye corners is not necessarily the eye center even for a frontal image. The second correction compensates for the fact that the eyeball center does not, in general, lie in the plane of the eye corners. In Equation (3), (ϕ_x, ϕ_y) is the head pose.

4. The radius of the eyeball in the image is computed $R = SR_0$.

2.0.2 Estimating the Gaze Direction

The gaze direction (θ_x, θ_y) can then be computed as follows (see Figure 1(d)):

$$\begin{pmatrix} \sin\theta_x \\ \sin\theta_y \end{pmatrix} = \begin{pmatrix} \frac{p_x - o_x}{\sqrt{R^2 - (p_y - o_y)^2}} \\ \frac{p_y - o_y}{\sqrt{R^2 - (p_x - o_x)^2}} \end{pmatrix} \tag{4}$$

2.0.3 Training the Anatomical Constants

The anatomical constants R_0, (T_x, T_y), and L are pre-computed in an offline training phase as follows. Substituting Equation (3) into Equation (4) gives:

$$\begin{pmatrix} \sin\theta_x \\ \sin\theta_y \end{pmatrix} = \begin{pmatrix} \frac{p_x - m_x - ST_x \cos\phi_x - SL\sin\phi_x}{\sqrt{(SR_0)^2 - (p_y - o_y)^2}} \\ \frac{p_y - m_y - ST_y \cos\phi_y - SL\sin\phi_y}{\sqrt{(SR_0)^2 - (p_x - o_x)^2}} \end{pmatrix} \tag{5}$$

We collect a set of training samples where the gaze direction and head pose of a person takes one of the two following special forms:

$$(\theta_x, \theta_y, \phi_x, \phi_y) = (\alpha_x^i, 0, \beta_x^i, 0)$$

and:

$$(\theta_x, \theta_y, \phi_x, \phi_y) = (0, \alpha_y^j, 0, \beta_y^j).$$

Suppose we have N_x images of the first form and N_y of the second, we combine the equations for these training samples and create the following matrix equation:

$$\begin{pmatrix} \frac{p_x^1 - m_x^1}{S_1} \\ \frac{p_x^2 - m_x^2}{S_2} \\ \vdots \\ \frac{p_x^{N_x} - m_x^{N_x}}{S_{N_y}} \\ \frac{p_y^1 - m_y^1}{S_1} \\ \frac{p_y^2 - m_y^2}{S_2} \\ \vdots \\ \frac{p_y^{N_y} - m_y^{N_y}}{S_{N_y}} \end{pmatrix} = \begin{pmatrix} \sin\alpha_x^1 & \sin\beta_x^1 & \cos\beta_x^1 & 0 \\ \sin\alpha_x^2 & \sin\beta_x^2 & \cos\beta_x^2 & 0 \\ \vdots & \vdots & \vdots & \vdots \\ \sin\alpha_x^{N_x} & \sin\beta_x^{N_x} & \cos\beta_x^{N_x} & 0 \\ \sin\alpha_y^1 & \sin\beta_y^1 & 0 & \cos\beta_y^1 \\ \sin\alpha_y^2 & \sin\beta_y^2 & 0 & \cos\beta_y^2 \\ \vdots & \vdots & \vdots & \vdots \\ \sin\alpha_y^{N_y} & \sin\beta_y^{N_y} & 0 & \cos\beta_y^{N_y} \end{pmatrix} \begin{pmatrix} R_0 \\ L \\ T_x \\ T_y \end{pmatrix}. \quad (6)$$

The least squares solution of this equation gives (R_0, L, T_x, T_y).

3 Driver Gaze Estimation with an Active Appearance Model

The usual approach to locating the inner and outer eye corners is feature point detection and tracking [4, 5]. The problem with these feature-based methods is that they are very local; they only use information in the immediate vicinity of the feature. Hence, feature point tracking is neither as robust nor as accurate as it could be. We now describe an approach that tracks the head as a single object and show how it can be used to: (1) estimate the head pose, (2) estimate the eye corner locations, and (4) extract the eye region for pupil localization.

3.1 Active Appearance Models

Active Appearance Models (AAMs) [2] are generative face models. An AAM consists of two components, the shape and the appearance. The *2D shape* of an AAM is defined by a 2D triangulated mesh and in particular the vertex locations of the mesh:

$$\mathbf{s} = \begin{pmatrix} u_1 & u_2 & \dots & u_n \\ v_1 & v_2 & \dots & v_n \end{pmatrix}. \tag{7}$$

AAMs allow linear shape variation. This means that the shape matrix $\mathbf{s}$ can be expressed as a base shape $\mathbf{s}_0$ plus a linear combination of m shape matrices $\mathbf{s}_i$:

$$\mathbf{s} = \mathbf{s}_0 + \sum_{i=1}^{m} p_i \, \mathbf{s}_i \tag{8}$$

where the coefficients p_i are the shape parameters. AAMs are normally computed from training data consisting of a set of images with the shape mesh (usually hand) marked on them [2]. The Iterative Procrustes Algorithm and Principal Component Analysis are then applied to compute the the base shape $\mathbf{s}_0$ and the shape variation $\mathbf{s}_i$. An example of the base shape $\mathbf{s}_0$ and the first two shape modes ($\mathbf{s}_1$ and $\mathbf{s}_2$) of an AAM are shown in Figure 2(a)–(c).

The *appearance* of the AAM is defined within the base mesh $\mathbf{s}_0$. Let $\mathbf{s}_0$ also denote the set of pixels $\mathbf{u} = (u, v)^{\mathrm{T}}$ that lie inside the base mesh $\mathbf{s}_0$, a convenient abuse of terminology. The appearance of the AAM is then an image $A(\mathbf{u})$ defined over the pixels $\mathbf{u} \in \mathbf{s}_0$. AAMs allow linear appearance variation. This means that the appearance $A(\mathbf{u})$ can be expressed as a base appearance $A_0(\mathbf{u})$ plus a linear combination of l appearance images $A_i(\mathbf{u})$:

$$A(\mathbf{u}) = A_0(\mathbf{u}) + \sum_{i=1}^{l} \lambda_i \, A_i(\mathbf{u}) \tag{9}$$

where λ_i are the appearance parameters. As with the shape, the appearance images A_i are usually computed by applying PCA to the (shape normalized) training images [2]. An example of the base

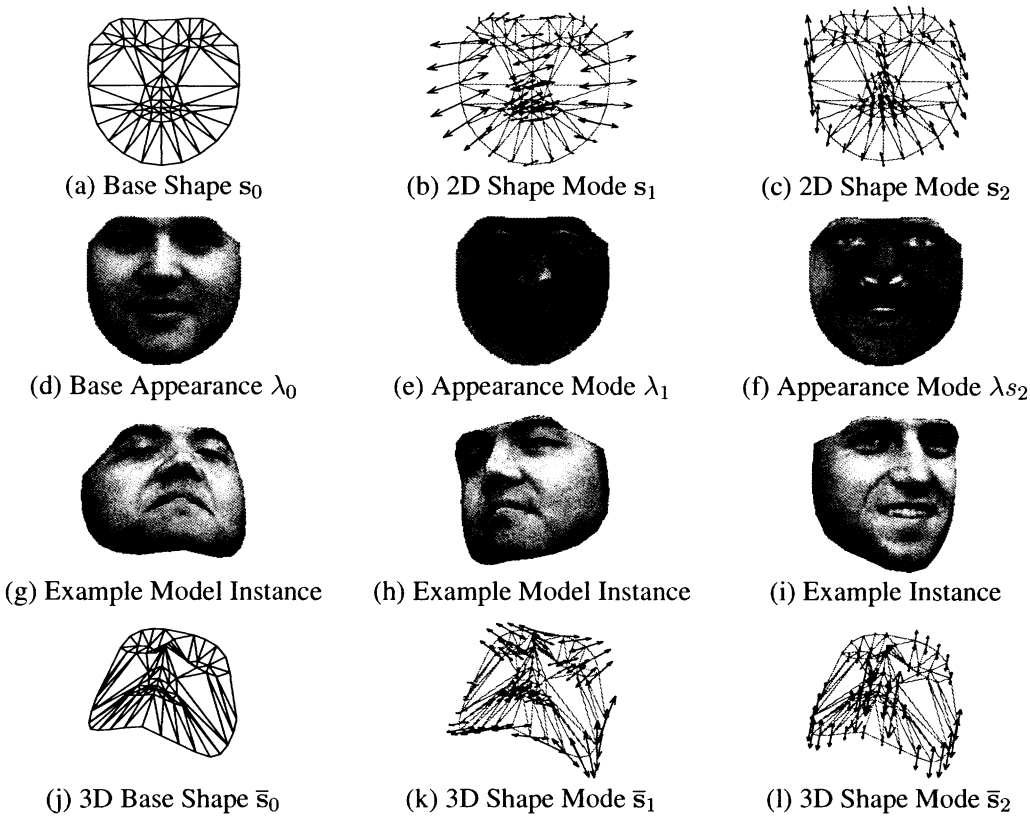

(a) Base Shape $\mathbf{s}_0$ (b) 2D Shape Mode $\mathbf{s}_1$ (c) 2D Shape Mode $\mathbf{s}_2$

(d) Base Appearance λ_0 (e) Appearance Mode λ_1 (f) Appearance Mode λs_2

(g) Example Model Instance (h) Example Model Instance (i) Example Instance

(j) 3D Base Shape $\bar{\mathbf{s}}_0$ (k) 3D Shape Mode $\bar{\mathbf{s}}_1$ (l) 3D Shape Mode $\bar{\mathbf{s}}_2$

Figure 2: An example Active Appearance Model [2]. (a–c) The AAM base shape $\mathbf{s}_0$ and the first two shape modes $\mathbf{s}_1$ and $\mathbf{s}_2$. (d–f) The AAM base appearance λ_0 and the first two shape modes λ_1 and λ_2. (g–i) Three model instances. (j–l) The base 3D shape $\bar{\mathbf{s}}_0$ and the first two 3D shape modes $\bar{\mathbf{s}}_1$ and $\bar{\mathbf{s}}_2$.

λ_0 and first two appearance modes (λ_1 and λ_2) are shown in Figures 2(d)–(f).

Although Equations (8) and (9) describe the AAM shape and appearance variation, they do not describe how to generate a *model instance.* The AAM model instance with shape parameters $\mathbf{p}$ and appearance parameters λ_i is created by warping the appearance A from the base mesh $\mathbf{s}_0$ to the model shape mesh $\mathbf{s}$. In particular, the pair of meshes $\mathbf{s}_0$ and $\mathbf{s}$ define a piecewise affine warp from $\mathbf{s}_0$ to $\mathbf{s}$ which we denote $\mathbf{W}(\mathbf{u};\mathbf{p})$. Three example model instances are included in Figures 2(g)–(i). This figure demonstrate the generative power of an AAM. The AAM can generate face images with different poses (Figures 2(g) and (h)), different identities (Figures 2(g) and (i)), and different expressions, (Figures 2(h) and (i)).

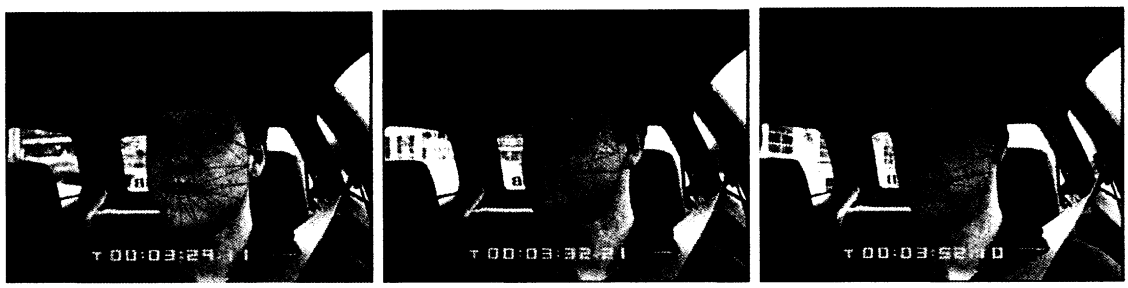

Figure 3: Example driver head tracking results with an AAM. View in color for the best clarity.

3.2 Real-Time Driver Head Tracking With an AAM

Driver head tracking is performed by "fitting" the AAM sequentially to each frame in the input video. Three frames from an example movie of a driver's head being tracked with an AAM are included in Figure 3. Given an input image I, the goal of AAM fitting is to minimize:

$$\sum_{\mathbf{u} \in \mathbf{s}_0} \left[A_0(\mathbf{u}) + \sum_{i=1}^{l} \lambda_i A_i(\mathbf{u}) - I(\mathbf{W}(\mathbf{u};\mathbf{p})) \right]^2 = \left\| A_0(\mathbf{u}) + \sum_{i=1}^{l} \lambda_i A_i(\mathbf{u}) - I(\mathbf{W}(\mathbf{u};\mathbf{p})) \right\|^2 \quad (10)$$

simultaneously with respect to the 2D AAM shape p_i and appearance λ_i parameters. In [6] we proposed an algorithm to minimize the expression in Equation (10) that operates at around 230 frames per second. For lack of space, the reader is referred to [6] for the details.

3.3 Estimating Driver Head Pose With an AAM

The shape component of an AAM is 2D which makes driver head pose estimation difficult. In order to extract the head pose, we also build a 3D linear shape model:

$$\overline{\mathbf{s}} = \overline{\mathbf{s}}_0 + \sum_{i=1}^{\overline{m}} \overline{p}_i \, \overline{\mathbf{s}}_i \quad (11)$$

where the coefficients $\overline{p}_i$ are the 3D shape parameters and $\overline{\mathbf{s}}$, etc, are the 3D shape coordinates:

$$\overline{\mathbf{s}} = \begin{pmatrix} x_1 & x_2 & \dots & x_n \\ y_1 & y_2 & \dots & y_n \\ z_1 & z_2 & \dots & z_n \end{pmatrix}. \tag{12}$$

In [11] we showed how the equivalent 3D shape variation $\overline{\mathbf{s}}_i$ can be computed from the corresponding 2D shape variation $\mathbf{s}_i$ using our non-rigid structure-from-motion algorithm [12]. An example of the 3D base shape $\overline{\mathbf{s}}_0$ and the first two 3D shape modes ($\overline{\mathbf{s}}_1$ and $\overline{\mathbf{s}}_2$) of the AAM in Figure 2 are shown in Figure 2(j)–(l). In order to combine this 3D model with the 2D model we need an image formation model. We use the weak perspective imaging model defined by:

$$\mathbf{u} = \mathbf{P}\mathbf{x} = \begin{pmatrix} i_x & i_y & i_z \\ j_x & j_y & j_z \end{pmatrix} \mathbf{x} + \begin{pmatrix} a \\ b \end{pmatrix}. \tag{13}$$

where (a, b) is an offset to the origin and the projection axes $\mathbf{i} = (i_x, i_y, i_z)$ and $\mathbf{j} = (j_x, j_y, j_z)$ are equal length and orthogonal: $\mathbf{i} \cdot \mathbf{i} = \mathbf{j} \cdot \mathbf{j}$; $\mathbf{i} \cdot \mathbf{j} = 0$. To extract the driver head pose and AAM scale we perform the AAM fitting by minimizing:

$$\left\| A_0(\mathbf{u}) + \sum_{i=1}^{l} \lambda_i A_i(\mathbf{u}) - I(\mathbf{W}(\mathbf{u};\mathbf{p})) \right\|^2 + K \cdot \left\| \mathbf{s}_0 + \sum_{i=1}^{m} p_i \, \mathbf{s}_i - \mathbf{P}\left(\overline{\mathbf{s}}_0 + \sum_{i=1}^{\overline{m}} \overline{p}_i \, \overline{\mathbf{s}}_i \right) \right\|^2 \tag{14}$$

simultaneously with respect to p_i, λ_i, $\mathbf{P}$, and $\overline{p}_i$, rather than using Equation (10). In Equation (14), K is a large constant weight. In [11] we extended our 2D AAM fitting algorithm [6] to minimize the expression in Equation (14). The algorithm operates at around 286Hz [11]. The second term enforces the (heavily weighted soft) constraints that the 2D shape $\mathbf{s}$ equals the projection of the 3D shape $\overline{\mathbf{s}}$ with projection matrix $\mathbf{P}$. Once the expression in Equation (14) has been minimized, the driver head pose and AAM scale can be extracted from the projection matrix $\mathbf{P}$. Two examples of pose estimation are shown in Figure 4.

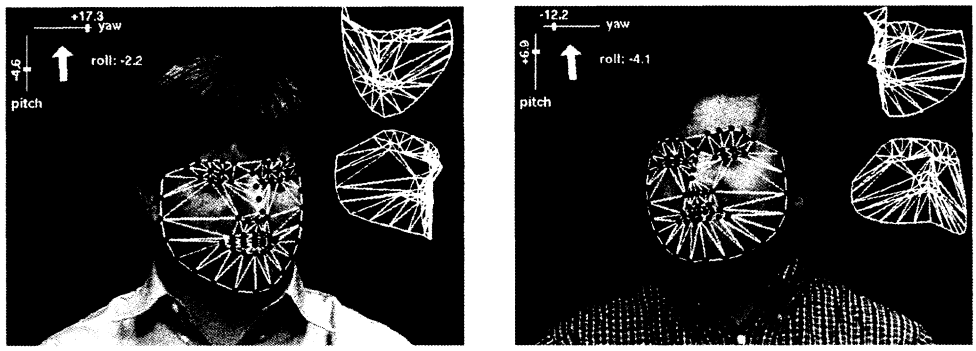

Figure 4: Pose estimation results. The computed roll, pitch, and yaw are displayed in the top left.

3.4 Eye Corner Tracking and Eye Region Extraction from an AAM

Once the AAM has been fit to an input video frame, it is easy to locate the eye corners and extract the eye regions. The AAM has mesh vertices that correspond to each of the inner and outer eye corners. The eye corner locations in the image can therefore be just read out of $\mathbf{W}(\mathbf{s};\mathbf{p})$, the location of the AAM mesh in the images. See Figure 5(a) for an example.

In the AAM, each eye is modeled by six mesh vertices. It is therefore also easy to extract the eye region as a box slightly larger than the bounding box of the six eye mesh vertices. If (x_i, y_i) denotes the six mesh vertices for $i = 1, \ldots, 6$, the eye region is the rectangle with bottom-left coordinate (BL_x, BL_y) and top-right coordinate (TR_x, TR_y), where:

$$\begin{pmatrix} BL_x \\ TR_x \\ BL_y \\ TR_y \end{pmatrix} = \begin{pmatrix} \min x_i \\ \max x_i \\ \min y_i \\ \max y_i \end{pmatrix} + \begin{pmatrix} -c_x \\ c_x \\ -d_y \\ d_y \end{pmatrix}. \tag{15}$$

and (c_x, d_y) is an offset to expand the rectangle. Again, see Figure 5(a) for an example.

3.5 Iris Detection

Once the eye region has been extracted from the AAM, we detect the iris to locate the center of the iris. Our iris detector is fairly conventional and consists of two parts. Initially template matching

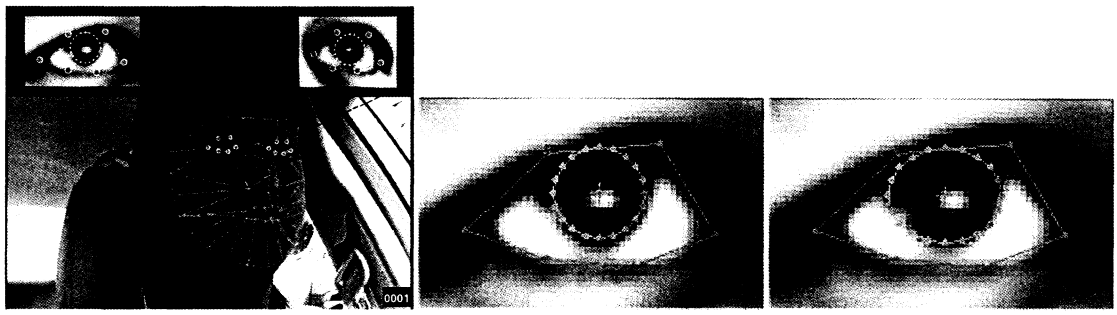

(a) Eye Region Extraction (b) Initial Iris Estimate (c) Refined Iris Estimate

Figure 5: Example iris detection result: (a) Example eye corner tracking and eye region extraction results computed from an AAM fit. (b) The initial iris location and radius computed by template matching. (c) The refined iris location and radius after edge-based ellipse fitting.

with a disk shaped template is used to approximately locate the iris. The iris location is then refined using an ellipse fitting algorithm similar to the ones in [7, 10].

3.5.1 Template Matching

We apply template matching twice to each of the eye regions using two different templates. The first template is a black disk template which is matched against the intensity image. The second template is a ring (annulus) template that is matched against the vertical edge image. The radius of both templates are determined from the scale of the AAM fit. The two sets of matching scores are summed to give a combined template matching confidence. The position of the pixel with the best confidence becomes the initial estimate of the center of the iris. In Figure 5(b) we overlay the eye image with this initial estimate of the iris location and radius.

3.5.2 Edge-Based Iris Refinement

The initial iris estimate is then refined as follows. First, edges are detected by scanning radially from the initial center of the pupil outward. Next, an ellipse is fit to the detected edges to refine the estimate of the iris center. Edges a long way away from the initial estimate of the radius are filtering out for robustness. The ellipse is parameterized:

$$a_1 x^2 + a_2 xy + a_3 y^2 + a_4 x + a_5 y = 1 \tag{16}$$

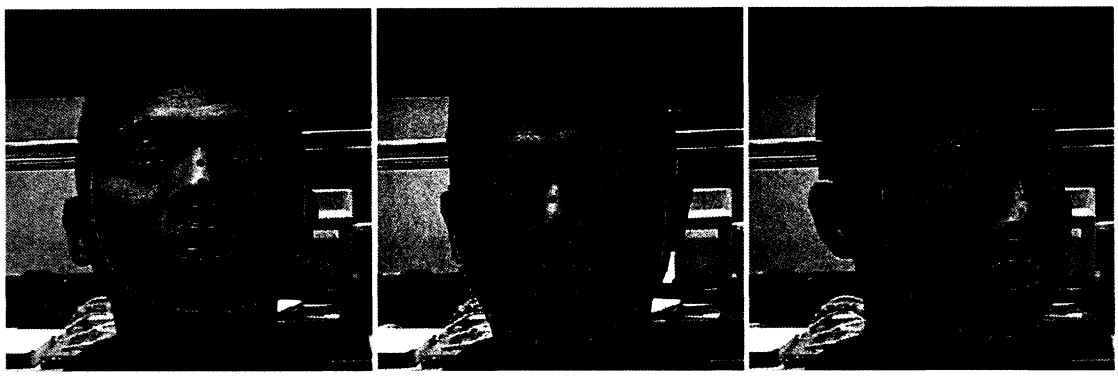

Figure 6: An example of head tracking with an AAM.

and the parameters $a_1, \ldots, a_5$ are fit using least squares. This refinement procedure is repeated iteratively until the estimate of the center of the iris converges (typically only 2-3 iterations are required.) Example results are shown in Figure 5(c).

4 Quantitative Evaluation in the Laboratory

4.1 AAM Fitting, Eye Corner Tracking, Pose and Scale Estimation

In Figure 6 we include three frames of a head being tracked using an AAM. Notice how the facial features are tracked accurately across wide variations in the head pose. In Figure 7 we include three example pose estimates using the 3D AAM. Note that the yaw is estimated particularly accurately. Besides the eye corner locations and the head pose, the other quantity we extract from the AAM fit is the head scale S. We evaluate the scale estimate using the fact that the scale is inversely proportional to the distance to the head (the depth.) In Figure 8 we compute the distance to the head using the scale as the driver slides the seat back.

4.2 Gaze Estimation

We collected a ground-truthed dataset by asking each subject to look in turn at a collection of markers on the wall. The 3D position of these markers was then measured relative to the head position and the ground-truth gaze angles computed. We took multiple sequences with different

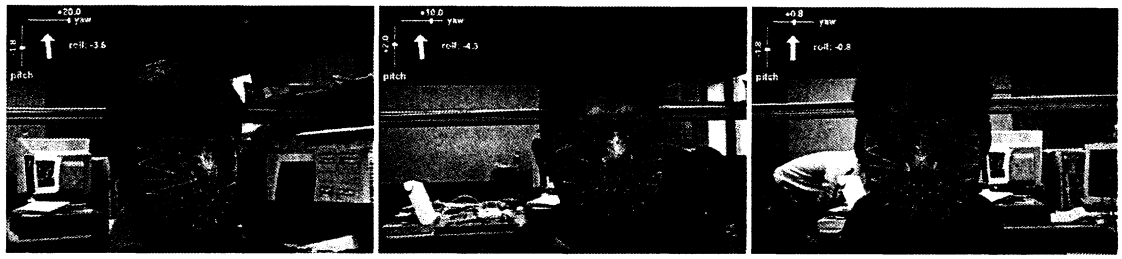

(a) Ground truth $(20, 0, 0)$ Result value $(20, -1.8, -3.6)$

(b) Ground truth $(10, 0, 0)$ Result value $(10, 2.0, -4.3)$

(c) Ground truth $(0, 0, 0)$ Result value $(0.8, -1.8, -0.8)$

Figure 7: Example pose (yaw, pitch, roll) estimation with the AAM.

(a) depth:64.7cm (b) depth:67.4cm (c) depth:71.3cm (d) depth:74.0cm

(e) depth:75.7cm (f) depth:77.5cm (g) depth:78.7cm (h) depth:80.1cm

Figure 8: Verification of the scale estimated by the AAM. Since the scale is inversely proportional to depth, we can use the scale to estimate the distance to the driver's head. (a-h) The distance estimated from the AAM scale increases smoothly as the seat is moved backward.

head poses. All variation was in the yaw direction and ranged from approximately -20 degrees to +20 degrees relative to frontal. In Figure 9(a–c) we include an example frontal images for each of 3 subjects. We overlay the image with the AAM fit and a line denoting the estimated gaze direction. We also include close ups of the extracted eye regions and the detected iris. In Figure 9(d–e) we plot the estimated azimuth gaze angle against the ground truth. The average error is 3.2 degrees. The green line in the figure denotes the "correct answer."

(a) Gaze of Subject 1 (b) Gaze of Subject 2 (c) Gaze of Subject 3

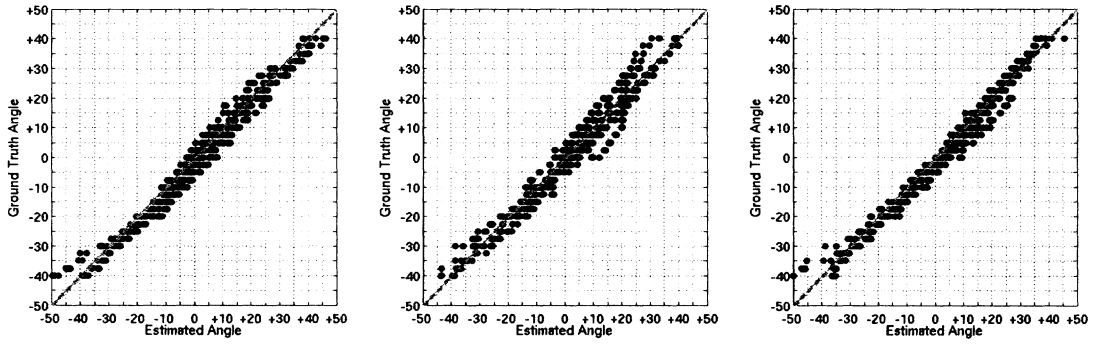

(d) Azimuth of subject 1 (e) Azimuth of subject 2 (f) Azimuth of subject 3

Figure 9: Gaze estimation. (a-c) Gaze estimates overlaid on the input image. We also include the AAM, the extracted eye region, and the detected iris. (d-f) A comparison between the ground-truth azimuth gaze angle and the angle estimated by our algorithm. The average error is 3.2 degrees.

5 Qualitative Evaluation in a Real-Car

If there are two cameras in the car, one imaging the driver, the other imaging the outside world, it is possible to calibrate the relative orientations of the camera by asking a person to look at a collection of points in the world and then marking the corresponding points in the outside-view image. The relative orientation can then be solved using least-squares. We performed this experiment and then asked the subject to track a person walking outside the car with their gaze. Three frames from a video of the results are shown in Figure 10. In Figures 10(a–c) we display the exterior view. We overlay the estimated gaze direction with a yellow circle than corresponds to a 5.0 degree gaze radius. In Figures 10(d–e) we include the corresponding interior view of the driver overlaid with the AAM, the extracted eye regions, the detected iris, and the estimated gaze plotted as a line. As can be seen, the person always lies well inside the circle, demonstrating the high accuracy of our algorithm.

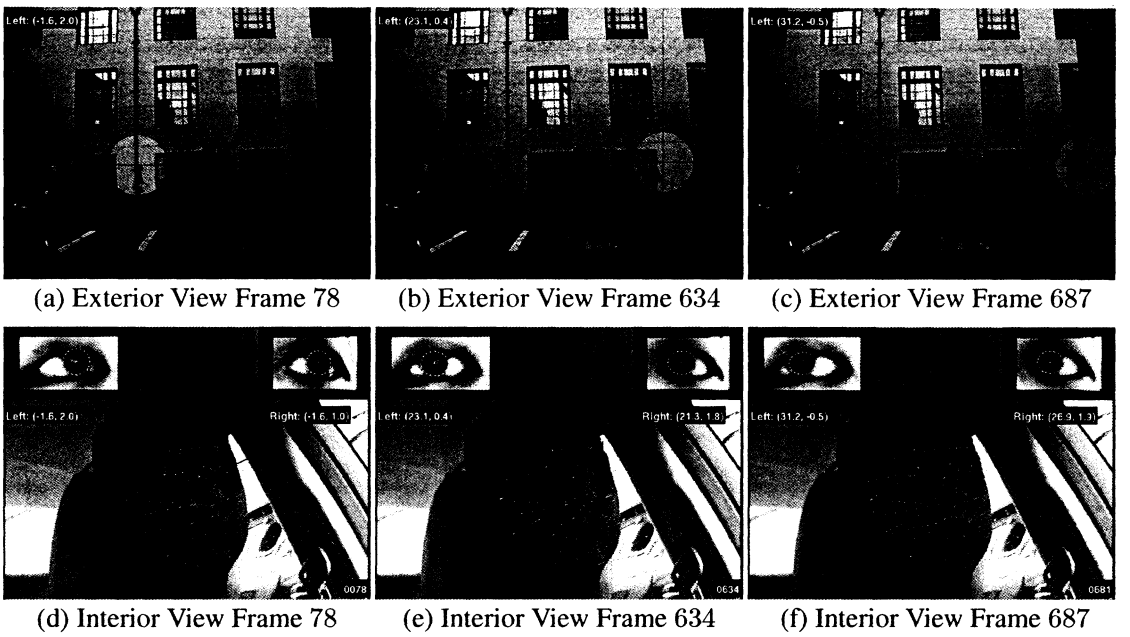

(a) Exterior View Frame 78 (b) Exterior View Frame 634 (c) Exterior View Frame 687

(d) Interior View Frame 78 (e) Interior View Frame 634 (f) Interior View Frame 687

Figure 10: Mapping the driver's gaze into the external scene. The driver was told to follow the person walking outside in the parking lot. We overlay the external view with a yellow circle with radius corresponding to a 5.0 error in the gaze estimated. As can be seen, the person always lies well within the circle demonstrating the accuracy of our algorithm.

6 Conclusion

We have presented a driver gaze estimation algorithm that uses an Active Appearance Model [2] to: (1) track the eye corners, (2) extract the eye region, (3) estimate the scale of the face, and (4) estimate the head pose. The irises are detected in the eye region using fairly standard techniques and the gaze estimated from the above information using a fairly standard geometric model. The robustness and accuracy of our passive, monocular system are derived from the AAM tracking of the whole head, rather than using a local feature based technique. Once the eye corners have been located, finding the irises and computing the gaze are straightforward.

Acknowledgments

The research described in this paper was supported by Denso Corporation, Japan.

References

[1] V. Blanz and T. Vetter. A morphable model for the synthesis of 3D faces. In *Proceedings of Computer Graphics, Annual Conference Series (SIGGRAPH)*, pages 187–194, 1999.

[2] T. Cootes, G. Edwards, and C. Taylor. Active appearance models. *IEEE Transactions on Pattern Analysis and Machine Intelligence*, 23(6):681–685, June 2001.

[3] A. Gee and R. Cipolla. Determining the gaze of faces in images. *Image and Vision Computing*, 30:63–647, 1994.

[4] J. Heinzmann and A. Zelinsky. 3-D facial pose and gaze point estimation using a robust real-time tracking paradigm. In *Proceedings of the IEEE International Conference on Automatic Face and Gesture Recognition*, pages 142–147, 1998.

[5] Y. Matsumoto and A. Zelinsky. An algorithm for real-time stereo vision implementation of head pose and gaze direction measurement. In *Proceedings of the IEEE International Conference on Automatic Face and Gesture Recognition*, pages 499–505, 2000.

[6] I. Matthews and S. Baker. Active Appearance Models revisited. *International Journal of Computer Vision*, 2004. (Accepted subject to minor revisions, Previously appeared as CMU Robotics Institute Technical Report CMU-RI-TR-03-02).

[7] T. Ohno, N. Mukawa, and A. Yoshikawa. FreeGaze: A gaze tracking system for everyday gaze interaction. In *Proceedings of the Symposium on ETRA*, pages 125–132, 2002.

[8] S. Romdhani and T. Vetter. Efficient, robust and accurate fitting of a 3D morphable model. In *Proceedings of the International Conference on Computer Vision*, 2003.

[9] P. Smith, M. Shah, and N. da Vitoria Lobo. Monitoring head/eye motion for driver alertness with one camera. In *Proceedings of the IEEE International Conference on Pattern Recognition*, pages 636–642, 2000.

[10] K. Talmi and J. Liu. Eye and gaze tracking for visually controlled interactive stereoscopic displays. In *Signal Processing: Image Communication 14*, pages 799–810, 1999.

[11] J. Xiao, S. Baker, I. Matthews, and T. Kanade. Real-time combined 2D+3D active appearance models. In *Submitted to the IEEE Conference on Computer Vision and Pattern Recognition*, 2004.

[12] J. Xiao, J. Chai, and T. Kanade. A closed-form solution to non-rigid shape and motion recovery. In *Proceedings of the European Conference on Computer Vision*, 2004.